The coated substrates were left at room temperature for 30 min before being subjected to controlled-humidity steaming at 150 °C. The steaming was done in the same reactor described previously [16].

The coated film was examined using atomic force microscopy (AFM, SEIKO SPA-400), UV-vis spectroscopy (Jasco-V-530), contact-angle measurement (KYAMO CA-D), and XRD (SHIMADZU XRD-6000) as well as the BL17A1 line of synchrotron radiation in NSRRC, Taiwan.

[1] G. A. Ozin, A. Kuperman, A. Stein, *Angew. Chem. Int. Ed. Engl.* **1989**, *28*, 359.
[2] L. Werner, J. Caro, G. Finger, J. Kornatowski, *Zeolites* **1992**, *12*, 658.
[3] F. Marlow, K. Hoffmann, W. Hill, J. Kornatowski, J. Caro, *Stud. Surf. Sci. Catal.* **1994**, *84*, 2277.
[4] F. Marlow, J. Kornatowski, B. Reck, I. Leike, K. Hoffmann, J. Caro, *Mol. Cryst. Liq. Cryst.* **1996**, *276*, 295.
[5] S. Megelski, G. Calzaferri, *Adv. Funct. Mater.* **2001**, *11*, 277.
[6] G. Calzaferri, S. Huber, H. Maas, C. Minkowski, *Angew. Chem. Int. Ed.* **2003**, *42*, 3732.
[7] I. Braun, G. Ihlein, F. Laeri, J. U. Nockel, G. Schulzekloff, F. Schueth, U. Vietze, O. Weiss, D. Wohrle, *Appl. Phys. B* **2000**, *70*, 335.
[8] F. F. Gao, G. S. Zhu, X. T. Li, B. S. Li, O. Terasaki, S. L. Qiu, *J. Phys. Chem. B* **2001**, *105*, 12 704.
[9] K. T. Jung, Y. G. Shul, *Chem. Mater.* **1997**, *9*, 420.
[10] J. Hedlund, S. Mintova, J. Sterte, *Microporous Mesoporous Mater.* **1999**, *28*, 185.
[11] Z. Wang, J. Hedlund, J. Sterte, *Microporous Mesoporous Mater.* **2002**, *52*, 191.
[12] K. Ha, Y. J. Lee, H. J. Lee, K. B. Yoon, *Adv. Mater.* **2000**, *12*, 1114.
[13] J. S. Lee, Y. J. Lee, E. L. Tae, Y. S. Park, K. B. Yoon, *Science* **2003**, *301*, 818.
[14] L. M. Huang, Z. B. Wang, J. Y. Sun, L. Miao, Q. Z. Li, Y. S. Yan, D. Y. Zhao, *J. Am. Chem. Soc.* **2000**, *122*, 3530.
[15] S. P. Naik, J. C. Chen, A. S. T. Chiang, *Microporous Mesoporous Mater.* **2002**, *54*, 293.
[16] S. P. Naik, A. S. T. Chiang, R. W. Thompson, *J. Phys. Chem. B* **2003**, *107*, 7006.
[17] S. P. Naik, A. S. T. Chiang, R. W. Thompson, F. C. Huang, H. M. Kao, *Microporous Mesoporous Mater.* **2003**, *60*, 213.
[18] R. A. Munoz, D. Beving, Y. S. Yan, *Ind. Eng. Chem. Res.* **2005**, *44*, 4310.

# Luminescent Carbon Nanotubes by Surface Functionalization**

By *Donglu Shi,* * *Jie Lian*, *Wei Wang*, *Guokui Liu*, *Peng He*, *Zhongyun Dong*, *Lumin Wang*, and *Rodney C. Ewing*

Surface functionalization of carbon nanotubes is an effective way of improving the solubility and dispersion of the nanotubes in aqueous solutions and to design new hybrid materials by coupling the properties of novel nanostructures to the carbon nanotubes.[1–4] Functionalization of carbon nanotubes can be achieved either by covalent or non-covalent methodologies.[5–9] The attachment of metal nanoparticles, particularly Au nanoparticles, to functionalized carbon nanotubes has recently been an active field of research for gas-sensor and catalytic applications.[10–14] In addition, various biological applications of the functionalized carbon nanotubes have been proposed, such as DNA[15] and protein biosensors,[8,16] biocatalysts, and bioseparators.[17]

Nanoparticles and nanotubes also find potential applications in the fields of cancer diagnosis and therapy. In the diagnosis and treatment of cancer, nanoparticles not only need a 'cavity' structure for the storage and delivery of drugs, but must also be luminescent in order to track and diagnose the effectiveness of the treatment. Nanoparticles or nanotubes can be functionalized for the qualitative or quantitative detec-

[*] Prof. D. L. Shi, W. Wang
Department of Chemical and Materials Engineering
University of Cincinnati
Cincinnati, OH 45221 (USA)
E-mail: shid@email.uc.edu
Dr. J. Lian, Prof. L. M. Wang, Prof. R. C. Ewing
Departments of Geological Sciences
Nuclear Engineering and Radiological Sciences
and Materials Science & Engineering
University of Michigan
Ann Arbor, MI 48109 (USA)
Dr. G. K. Liu
Chemistry Division
Argonne National Laboratory
Argonne, IL 60439 (USA)
P. He
Department of Mechanical Engineering
University of Cincinnati
Cincinnati, OH 45221 (USA)
Prof. Z. Dong
Department of Internal Medicine, College of Medicine
University of Cincinnati
Cincinnati, OH 45221 (USA)

WILEY InterScience
DISCOVER SOMETHING GREAT

tion of tumor cells. However, targeting cancer cells and the delivery of drugs to localized regions remains a challenge in cancer therapy. Thus, the design of novel nanostructures with multifunctionalities, such as fluorescent signaling, biolinkers, biocompatibility, and drug-carrying capability, is the key to the success of this application. A nanotube may be considered as a 'reservoir' for the containment of anticancer drugs. Multiwalled carbon nanotubes (MWCNTs) have a hollow structure with inner diameters of the order of 100 nm, which is an ideal geometry for drug transport and delivery. However, carbon nanotubes have only been observed to exhibit weak infrared (IR) emissions.[18] For diagnosis, the nanotubes must be functionalized with spectroscopically characteristic fluorescent dyes.[19] One of the novel approaches in biomarking is through targeting cancer cells with luminescent nanoparticles, such as quantum dots.[20–24] Compared with traditional organic fluorophores, quantum dots have superior properties, which include a higher quantum yield and much sharper emission spectra.

Here, a novel approach to design luminescent carbon nanotubes by depositing europium-doped $Y_2O_3$ nanophosphors onto the surfaces of MWCNTs is presented. The surface morphologies and microstructure have been characterized by high-resolution transmission electron microscopy (HRTEM) and electron diffraction spectroscopy (EDS). Fluorescent spectrometer measurements confirm that the surface-functionalized MWCNTs exhibit luminescence in the visible light range. This method opens up the possibility of designing functionalized carbon nanotubes for cancer diagnosis and treatment by attaching nanoparticles that are luminescent over a desired optical range. Therefore, the functionalized MWCNTs can be used simultaneously as drug carriers and biomarkers.
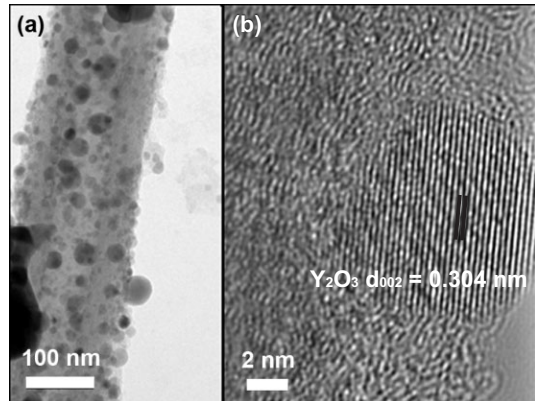
Figure 1a shows a bright-field TEM image of a MWCNT surface functionalized with an Eu-doped $Y_2O_3$ film heat treated at 650 °C. The outer surface of the nanotube is uniformly coated by a thin film of 10 nm. Crystallites that show a dark contrast with a particle size of ~5 nm were observed to be embedded in the coated thin film. The inset in Figure 1a is the selected-area electron diffraction (SAED) pattern acquired from the surface-functionalized carbon nanotubes. The diffuse diffraction arc corresponds to diffraction from the (002) graphite layers of the carbon nanotubes. The diffraction pattern can be indexed using structural data of $Y_2O_3$ crystals described by a hexagonal unit cell. The HRTEM image (Fig. 1b) of a nanoparticle grown at the nanotube surface and the corresponding Fourier-filtered transformed (FFT) image can be consistently indexed from the same $Y_2O_3$ structure. The EDS measurements (Fig. 1c) indicate the major elements carbon, yttrium, and europium on the nanotube surface, which are consistent with the coating process and TEM observations. These results suggest the identity of the nanoparticle as Eu-doped $Y_2O_3$. A HRTEM image (Fig. 1d) clearly shows the crystalline features of the coating film on the outside surface of a carbon nanotube. The (002) lattice plane of the graphitic interlayer of the carbon nanotube was evident. The morphology of the surface coating changes dramatically as the heat-treatment temperature increases from 650 to 950 °C (Fig. 2). The surface coating ap-
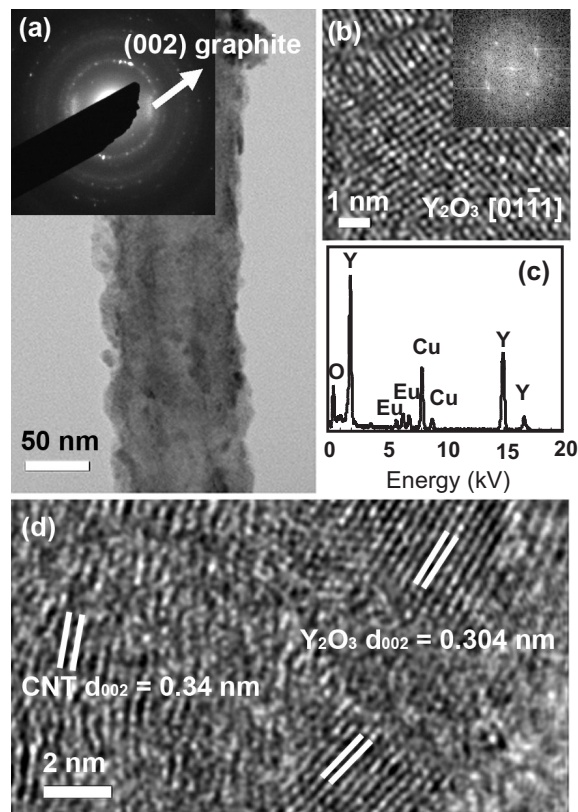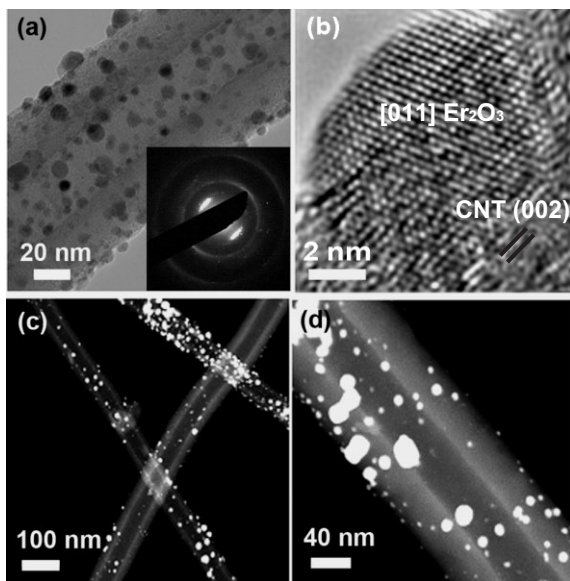


**Figure 1.** a) A bright-field TEM image showing the deposition of an Eu-doped $Y_2O_3$ film on a MWCNT heat treated at 650 °C. The inset is the selected-area electron diffraction (SAED) pattern acquired from carbon nanotubes and the coated film. b) A HRTEM image shows that the nanoparticles dispersed into the coating film are $Y_2O_3$, based on the lattice fringe spacings and Fourier-filtered transformed (FFT) image (inset in (b)), and this is consistent with the EDS spectrum (c). d) HRTEM images showing crystalline Eu-doped $Y_2O_3$ on a nanotube heat treated at 650 °C. The (002) lattice planes of the graphitic interlayer are clearly shown.

pears to be transformed from a uniform thin film (Fig. 1a) to well-dispersed, nanometer-sized nuclei. These nuclei are spheroidal in shape as a result of the high-temperature treatment (Fig. 2a). The spheroidal crystals appear to be deeply embedded in the nanotube wall and are therefore strongly bonded to it. It is essential that these luminescent particles do not separate from the nanotube substrate during transport in bodily fluids. The EDS results show a similar chemistry as compared with its counterpart, which was heat treated at 650 °C.

In order to investigate the effects of yttrium concentration on the surface deposition and optical properties of the surface-functionalized MWCNTs, pure $Er_2O_3$ was also deposited on the nanotube surfaces. The procedure was the same as that used for depositing Eu-doped $Y_2O_3$ on the nanotubes. After drying, the $Er_2O_3$-coated nanotubes were heat treated at 650 °C for 24 h. Well-dispersed nanoparticles were observed on the nanotube surfaces (Fig. 3). The particle size was typically 5–20 nm with a 'rounded' morphology. These crystallites not only exhibit clear lattice fringes, but also distinct boundaries

**Figure 2.** a) A bright-field TEM image and b) HRTEM image showing the surface deposition of an Eu-doped $Y_2O_3$ film on MWCNTs, heat treated at 950 °C.



**Figure 3.** a) A bright-field TEM image showing the deposition of $Er_2O_3$ nanoparticles on the surface of a carbon nanotube heat treated at 650 °C. The $Er_2O_3$ nanoparticles are well dispersed on the outside surface. The diffraction pattern (inset) can be indexed as cubic $Er_2O_3$. b) A HRTEM image showing an $Er_2O_3$ nanoparticle with an orientation of [011] absorbed at the side wall of a carbon nanotube. The (002) graphitic interlayer can be seen clearly. c,d) Z-contrast images showing $Er_2O_3$ deposition on the surface of MWCNTs. The $Er_2O_3$ nanoparticles show some non-uniformity in grain size, which varies from 30 nm to a few nanometers.

within the carbon matrix. Both the HRTEM image (Fig. 3b) and SAED results (inset in Fig. 3a) indicate that these nanoparticles are cubic $Er_2O_3$. Figures 3c,d show the high-angle annular dark-field scanning transmission electron microscopy (STEM) images (Z-contrast) of the nanotube surfaces coated by $Er_2O_3$ nanoparticles. Owing to the high atomic mass, the $Eu_2O_3$ nanoparticles display bright contrast in the Z-contrast image. The EDS spectra show distinctive features between the 'naked' and coated nanotubes, the former contains only carbon

while the latter exhibits strong signals of erbium. A non-uniform distribution of nanoparticles was evident among the different carbon nanotubes and at different locations.

Under a 355 nm pulsed-laser excitation, $Eu^{3+}$ luminescence was observed at room temperature from samples of the coated MWCNTs heat treated at 650 and 950 °C (Fig. 4). As shown in Figures 4a,b the emission lines are characteristic of the $Eu^{3+}$ $^5D_0$–$^7F_J$ ($J = 0$, 1, 2) electronic transitions. The efficiency of luminescence emission from the sample treated at 950 °C is much higher than that from the sample treated at 650 °C. The sharp lines in the emission spectrum of the sample treated at 950 °C indicate that $Eu^{3+}$ doped in $Y_2O_3$ has a well-
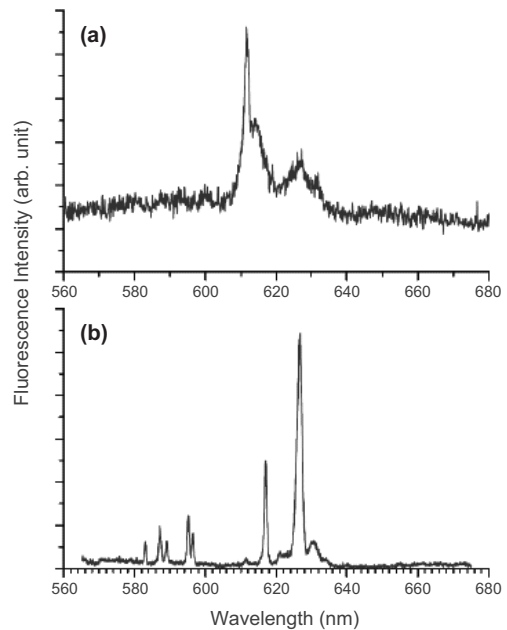


**Figure 4.** Luminescence emission spectra of Eu-doped $Y_2O_3$-coated MWCNTs heat treated at a) 650 and b) 950 °C.

defined crystalline structure, whereas the broader spectrum of the sample treated at 650 °C suggests a more disordered atomic-scale structure. No visible luminescence was observed at room temperature from the nanotubes coated with $Er_2O_3$. Quenching of $Er^{3+}$ fluorescence is expected due to $Er^{3+}$–$Er^{3+}$ interactions and energy transfer between the $Er_2O_3$ nanoparticles and the MWCNTs. However, IR fluorescence at a wavelength of 1.5 μm and longer was detected with an IR photon detector. For $Eu^{3+}/Y_2O_3$-coated carbon nanotubes, in addition to the visible fluorescence from $Eu^{3+}$, IR emission with a wavelength longer than 1.2 μm was observed with 355 nm excitation. Similar IR emission was also observed in the carbon nanotubes without a $Eu^{3+}$ phosphor coating, which indicates that the IR emission is from the nanotubes. In comparison to the excitation emission from single-walled carbon nanotubes (SWCNTs) with energies from 1.21 to 1.36 eV,[18] the fluorescence emission from the nanotubes studied here are also luminescent, but at much lower energies.

For successful deposition of Eu-doped $Y_2O_3$ and surface functionalization, the Eu-doped $Y_2O_3$ particles should wet the nanotube surfaces with a minimum surface energy, $\gamma$. This leads to the Eu-doped $Y_2O_3$ particles forming a small dihedral angle $\delta$ with the MWCNT surfaces. Interfaces with small $\gamma$ may be confirmed by good atomic-scale structural match at the interface (Fig. 1d). It is assumed that the close-packed (002) plane of the $Y_2O_3$ hexagonal unit cell favors to lie on the (002) graphitic layer of the carbon nanotubes, which may lead to a reduction in $\delta$ and $\gamma$. Therefore, it is energetically favorable for the small $Y_2O_3$ particles to nucleate and grow on the MWCNT surfaces and to form a uniform film at the low temperature of 650 °C (Fig. 1). At a considerably higher temperature of 950 °C, the deposited Eu-doped $Y_2O_3$ particles tend to become more spherical to further minimize their surface energies. As can be seen in Figure 1, these nanoparticles are fine crystallites with an average diameter of ~5 nm at 650 °C. It should be noted that nanocrystallites of Eu-doped $Y_2O_3$ could only nucleate and grow on the nanotube substrate under a condition of heterogeneous nucleation. Owing to the relatively high energies during the initial stage of nucleation and growth, these fine crystallites are not energetically stable. At elevated temperatures (Fig. 2), they continue to grow. The growth of these fine crystallites requires mass transport towards them. Therefore, each crystallite may grow at the expense of the surface thin film, which leads to separate, dispersed, and larger (10–20 nm) nanoparticles of Eu-doped $Y_2O_3$. Interestingly, spheroidal particles occur at much lower temperatures, e.g., 650 °C, in the case of $Er_2O_3$ deposition on MWCNTs. As shown in Figure 3, the $Er_2O_3$ nanoparticles have a spherical shape, and the diffraction patterns indicate that $Er_2O_3$ is cubic. This suggests a considerable lattice mismatch between the $Er_2O_3$ nanoparticles and the MWCNT. This lattice mismatch will lead to an increased dihedral angle and will reduce the wetability. Hence, in contrast to Eu-doped $Y_2O_3$, it maybe difficult to deposit a uniform thin film on the nanotube surface, on the contrary pure $Er_2O_3$ tends to grow as individual spherical particles on the surface.

In summary, by depositing rare-earth-doped $Y_2O_3$ nano-phosphors onto the outside surfaces of MWCNTs, the carbon nanotubes exhibit luminescent emission in the visible-light range. The surface-functionalized carbon nanotubes may find important applications in novel optical devices that use carbon nanotubes as building blocks. This method can also be applied to the design of luminescent carbon nanotubes for the application of cancer diagnosis and treatment, by attaching optically active rare-earth nanoparticles or quantum dots that are luminescent over the desired optical range. Thus the functionalized MWCNTs can be used simultaneously as drug carriers and biomarkers.

## Experimental

Commercial-grade Pyrograf III MWCNTs were used as substrates [25]. The MWCNTs were 70–200 nm in diameter and several micrometers in length. Rare-earth-doped $Y_2O_3$ was deposited on the

MWCNTs by a solution method [26]. The carbon nanotubes were first acid treated for oxidation, and then dispersed in 250 mL of distilled water by ultrasonic vibration for 0.5 h and allowed to stabilize for 1 h. Certain volumes of the solutions containing europium and yttrium were added into the MWCNT suspension, and the mixture was vibrated for 0.5 h. Aqueous ammonia was added to the solution, and at least 10 h was allowed for incubation. The solution was heated at 80 °C to entirely evaporate the water. The temperature of the drying process was strictly controlled and the heating rate varied over different temperature ranges. The dried powder (a mixture of MWCNTs, $Y_2O_3$, and rare-earth elements) was subsequently heat treated at 650 and 950 °C for 12 h. The functionalized MWCNT surface structure and morphology were studied by using a JEOL 2010F transmission electron microscope. The TEM samples of MWCNTs were prepared by dispersing them directly on perforated carbon films supported with Cu grids. Laser spectroscopic experiments were completed in order to study the optical behavior of the functionalized MWCNTs.

[1] S. S. Wong, E. Joselevich, A. T. Woolley, C. L. Cheung, C. M. Lieber, *Nature* **1998**, *394*, 52.

[2] A. Hirsch, *Angew. Chem. Int. Ed.* **2002**, *41*, 1853.

[3] D. Shi, J. Lian, P. He, L. M. Wang, W. J. Van Ooij, M. Schulz, Y. J. Liu, D. B. Mast, *Appl. Phys. Lett.* **2002**, *81*, 5216.

[4] D. Shi, J. Lian, P. He, L. M. Wang, M. Schultz, D. B. Mast, *Appl. Phys. Lett.* **2003**, *83*, 5301.

[5] M. Zheng, A. Jagota, E. D. Semke, B. A. Diner, R. S. Mclean, S. R. Lustig, R. E. Richardson, N. G. Tassi, *Nat. Mater.* **2003**, *2*, 338.

[6] A. Star, D. Steuerman, J. R. Heath, J. F. Stoddart, *Angew. Chem. Int. Ed.* **2002**, *41*, 2508.

[7] C. Richard, F. Balavoine, P. Schultz, T. W. Ebbesen, C. Mioskowski, *Science* **2003**, *300*, 775.

[8] R. J. Chen, S. Bangsaruntip, K. A. Drouvalakis, N. W. S. Kam, M. Shim, Y. Li, W. Kim, P. J. Utz, H. J. Dai, *Proc. Natl. Acad. Sci. USA* **2003**, *100*, 4984.

[9] R. J. Chen, Y. Zhang, D. Wang, H. J. Dai, *J. Am. Chem. Soc.* **2001**, *123*, 3838.

[10] B. C. Satishkumar, E. M. Vogl, A. Govindaraj, C. N. R. Rao, *J. Phys. D* **1996**, *29*, 3173.

[11] K. Jiang, A. Eitan, L. S. Schadler, P. M. Ajayan, R. W. Siegel, N. Grobert, M. Mayne, M. Reyes-Reyes, H. Terrones, M. Terrones, *Nano Lett.* **2003**, *3*, 275.

[12] A. V. Ellis, K. Vijayamohanan, R. Goswami, N. Chakrapani, L. S. Ramanathan, P. M. Ajayan, G. Ramanath, *Nano Lett.* **2003**, *3*, 279.

[13] L. Jiang, L. Gao, *Carbon* **2003**, *41*, 2923.

[14] A. Fasi, I. Palinko, J. W. Seo, Z. Konya, K. Hernadi, I. Kiricsi, *Chem. Phys. Lett.* **2003**, *372*, 848.

[15] K. A. Williams, P. T. Veenhuizen, B. G. de la Torre, R. Eritja, C. Dekker, *Nature* **2002**, *420*, 761.

[16] J. J. Gooding, R. Wibowo, J. Q. Liu, W. R. Yang, D. Losic, S. Orbons, F. J. Mearns, J. G. Shapter, D. B. Hibbert, *J. Am. Chem. Soc.* **2003**, *125*, 9006.

[17] D. T. Mitchell, S. B. Lee, L. Trofin, N. Li, T. K. Nevanen, H. Soderlund, C. R. Martin, *J. Am. Chem. Soc.* **2002**, *124*, 11 864.

[18] F. Wang, G. Dukovic, L. E. Brus, T. F. Heinz, *Science* **2005**, *308*, 838.

[19] S. Park, T. A. Taton, C. A. Mirkin, *Science* **2002**, *295*, 1503.

[20] B. Dubertret, P. Skourides, D. J. Norris, V. Noireaux, A. H. Brivanlou, A. Libchaber, *Science* **2002**, *298*, 1759.

[21] X. Wu, H. Liu, J. Liu, K. N. Haley, J. A. Treadway, J. P. Larson, N. Ge, F. Peale, M. P. Bruchez, *Nat. Biotechnol.* **2003**, *21*, 41.

[22] J. K. Jaiswal, H. Mattoussi, J. M. Mauro, S. M. Simon, *Nat. Biotechnol.* **2003**, *21*, 47.

[23] E. B. Voura, J. K. Jaiswal, H. Mattoussi, S. M. Simon, *Nat. Med.* **2004**, *10*, 993.

[24] D. R. Larson, W. R. Zipfel, R. M. Williams, S. W. Clark, M. P. Bruchez, F. W. Wise, W. W. Webb, *Science* **2003**, *300*, 1434.

[25] Applied Sciences Inc., www.apsci.com.

[26] X. Y. Chen, L. Yang, R. E. Cook, S. Skanthakumar, D. Shi, G. K. Liu, *Nanotechnology* **2003**, *14*, 670.

# Defect-Mode Lasing with Lowered Threshold in a Three-Layered Hetero-Cholesteric Liquid-Crystal Structure**

By *Myoung Hoon Song*, *Na Young Ha*, *Kazuhiro Amemiya*, *Byoungchoo Park*, *Yoichi Takanishi*, *Ken Ishikawa*, *Jeong Weon Wu*, *Suzushi Nishimura*, *Takehiro Toyooka*, and *Hideo Takezoe**

Cholesteric liquid crystals (CLCs) are regarded as self-assembling one-dimensional (1D) photonic crystals (PCs). A helical structure is spontaneously formed to give a unique property called selective reflection; i.e., circularly polarized (CP) light having the same handedness as the CLC helix cannot propagate through the CLCs in a frequency range corresponding to the photonic bandgap (PBG).[1] This optical property provides us with promising photonic devices. The most extensively studied property has been lasing at the PBG edge, where the photon group velocity approaches zero.

[*] Prof. H. Takezoe, Dr. M. H. Song, K. Amemiya, Dr. Y. Takanishi, Prof. K. Ishikawa
Department of Organic and Polymeric Materials
Tokyo Institute of Technology
2-12-1 O-okayama, Meguro-ku, Tokyo 152-8552 (Japan)
E-mail: htakezoe@o.cc.titech.ac.jp
N. Y. Ha, Prof. J. W. Wu
Department of Physics
Ewha Womans University
Seoul 120-750 (Korea)
Prof. B. Park
Department of Electrophysics
Kwangwoon University
Seoul 139-701 (Korea)
Dr. S. Nishimura, T. Toyooka
Nippon Oil Corporation
Central Technical Research Laboratory
8 Chidori-cho, Naka-ku, Yokohama 231-0815 (Japan)

Many achievements have been reported in low-molecular-weight CLCs[2–6] and polymeric cholesteric liquid crystals (PCLCs).[7–9] For practical applications, continuous-wave lasing is desired. For this purpose, lowering the lasing threshold is indispensable, and extensive studies have been devoted to achieving this goal.[10,11] In this paper, we report a novel cavity structure for defect-mode lasing with a lowered threshold. The cell used consists of three CLC layers, the middle of which contains laser dyes and has the opposite handedness helix and a narrower PBG than those layers on either side. It was found that the defect states emerge, and the photonic density of state (DOS) is resonantly enhanced when the defect mode coincides with the edge mode. The lasing from this enhanced mode was found to show a lower threshold value.

In order to reduce the lasing threshold, the emission rate must be enhanced. According to Fermi's golden rule,[12] the emission rate $\omega_i$ for $i$ optical eigenmodes is expressed by

$$\omega_i \sim M_i \left| \mathbf{E}_i^* \cdot \mathbf{d} \right|^2 \tag{1}$$

where $\mathbf{E}_i$ and $M_i$ are an electric field and a DOS of the $i$th mode, respectively, and $\mathbf{d}$ is a transition dipole moment. Hence, the optimum situation is ascribed to two conditions: realization of 1) a uniform orientation of $\mathbf{d}$ parallel to $\mathbf{E}$, and 2) a high DOS. The first condition is equivalent to realizing highly ordered dye molecules along the local director of a nematic liquid crystal (NLC) host.[5,6,13] It is predicted that a high DOS and the consequent low-threshold lasing would occur at the defect modes within the PBG, since the photon dwell time is enhanced, and gives ample opportunity for amplification by stimulated emission.[14,15] The introduction of a quarter-wavelength space in the middle of a layered isotropic 1D sample produces a defect in the middle of the PBG and it is widely used to produce high-$Q$ laser cavities (where $Q$ is a variable that describes the sharpness of the resonance).[16] Moreover, several types of defects have been studied by the introduction of an isotropic spacing layer in the middle of the CLCs,[17] e.g., the creation of a phase jump without any spacing layer in the CLC[18] and smectic LC structures,[19] and the local deformation of the helix in the middle of the CLC layer.[20] The Bragg reflection was studied in a CLC Fabry–Perot cavity by adding a CLC layer between two distributed Bragg reflectors (DBRs).[21] Schmidtke et al. and Ozaki et al. demonstrated low-threshold defect-mode lasing by using a phase jump in CLCs.[22,23] Phase-retardation defect-mode lasing was also demonstrated by the construction of a cell composed of a dye-doped nematic defect layer sandwiched between PCLC films.[24] In this study, a sophisticated system comprising a dye-doped left-handed (L-) helical CLC sandwiched by two right-handed (R-) helical PCLC layers was constructed and low-threshold lasing was achieved.

The main cell structure of a R-PCLC/dye-doped L-CLC/R-PCLC three-layered cell is shown in Figure 1a. A two-layered cell (Fig. 1b) and a single-layered cell (a simple dye-doped L-CLC layer, not shown) were also used as references.